International Journal of Biological Macromolecules 247 (2023) 125701

Contents lists available at ScienceDirect

International Journal of Biological Macromolecules

journal homepage: www.elsevier.com/locate/ijbiomac

Polysaccharide-based nano-engineered multilayers for controlled cellular adhesion in label-free biosensors

Monika Wasilewska [a,*], Aneta Michna [a], Agata Pomorska [a], Karol Wolski [b], Szczepan Zapotoczny [b], Enikő Farkas [c], Zoltan Szittner [c], Inna Szekacs [c], Robert Horvath [c]

[a] Jerzy Haber Institute of Catalysis and Surface Chemistry, Polish Academy of Sciences, Niezapominajek 8, PL-30239 Krakow, Poland
[b] Faculty of Chemistry, Jagiellonian University, Gronostajowa 2, 30-387 Krakow, Poland
[c] Nanobiosensorics Laboratory, Institute of Technical Physics and Materials Science, Centre for Energy Research, 1121 Budapest, Hungary

ARTICLE INFO

Keywords:
Macroion multilayers
Polysaccharide layers
Label-free biosensors
Streaming potential
OWLS
Resonant waveguide grating
Cell adhesion
Antimicrobial coatings
Holomonitor
QCM

ABSTRACT

Controlling cellular adhesion is a critical step in the development of biomaterials, and in cell- based biosensing assays. Usually, the adhesivity of cells is tuned by an appropriate biocompatible layer. Here, synthetic poly (diallyldimethylammonium chloride) (PDADMAC), natural chitosan, and heparin (existing in an extracellular matrix) were selected to assembly PDADMAC/heparin and chitosan/heparin films. The physicochemical properties of macroion multilayers were determined by streaming potential measurements (SPM), quartz crystal microbalance (QCM-D), and optical waveguide lightmode spectroscopy (OWLS). The topography of the wet films was imaged using atomic force microscopy (AFM).

The adhesion of preosteoblastic cell line MC3T3-E1 on those well-characterized polysaccharide-based multilayers was evaluated using a resonant waveguide grating (RWG) based optical biosensor and digital holographic microscopy. The latter method was engaged to investigate long-term cellular behavior on the fabricated multilayers.

(PDADMAC/heparin) films were proved to be the most effective in inducing cellular adhesion. The cell attachment to chitosan/heparin–based multilayers was negligible. It was found that efficient adhesion of the cells occurs onto homogeneous and rigid multilayers (PDADMAC/heparin), whereas the macroion films forming "sponge-like" structures (chitosan/heparin) are less effective, and could be employed when reduced adhesion is needed.

Polysaccharide-based multilayers can be considered versatile systems for medical applications. One can postulate that the presented results are relevant not only for modeling studies but also for applied research.

1. Introduction

Cell adhesion plays an important role in the survival and function of the development of tissue. Transmembrane receptor integrins in a cell membrane mediate the adhesion process to connect a surface, another cell, or the extracellular matrix (ECM). ECM is a three-dimensional network consisting of various macromolecules (glycoproteins, collagens, glycosaminoglycans, and proteoglycans) that provides structural and biochemical support to surrounding cells and allows for the adhesion of the cells [1].

In the process of cell adhesion, the elastic cell membrane deforms and extends on the surface during the cell spreading. The disruption of integrin connections, i.e. detachment of cells from the surface, indicates the process of anoikis, that follows the cell death. This process occurs during inadequate cell growth and adhesion to a defective matrix. [2–5].

Control over the adhesion properties of surfaces is fundamental for tissue engineering, medical implant improvement, and the development of new drug delivery systems. In recent years, macroion multilayers (engineered self-assembled films) have received great attention as nanoscaffolds supporting cell adhesion, proliferation, and function [6,7]. A strategy allowing to produce macroion multilayer films, that can effectively bind cells is also a basis for the development of effective

* Corresponding author.
E-mail addresses: monika.wasilewska@ikifp.edu.pl (M. Wasilewska), aneta.michna@ikifp.edu.pl (A. Michna), agata.pomorska@ikifp.edu.pl (A. Pomorska), wolski@chemia.uj.edu.pl (K. Wolski), zapotocz@chemia.uj.edu.pl (S. Zapotoczny), farkas.eniko@ek-cer.hu (E. Farkas), szittner.zoltan@ek-cer.hu (Z. Szittner), szekacs.inna@ek-cer.hu (I. Szekacs), horvath.robert@ek-cer.hu (R. Horvath).

https://doi.org/10.1016/j.ijbiomac.2023.125701
Received 21 April 2023; Received in revised form 22 June 2023; Accepted 3 July 2023
Available online 8 July 2023

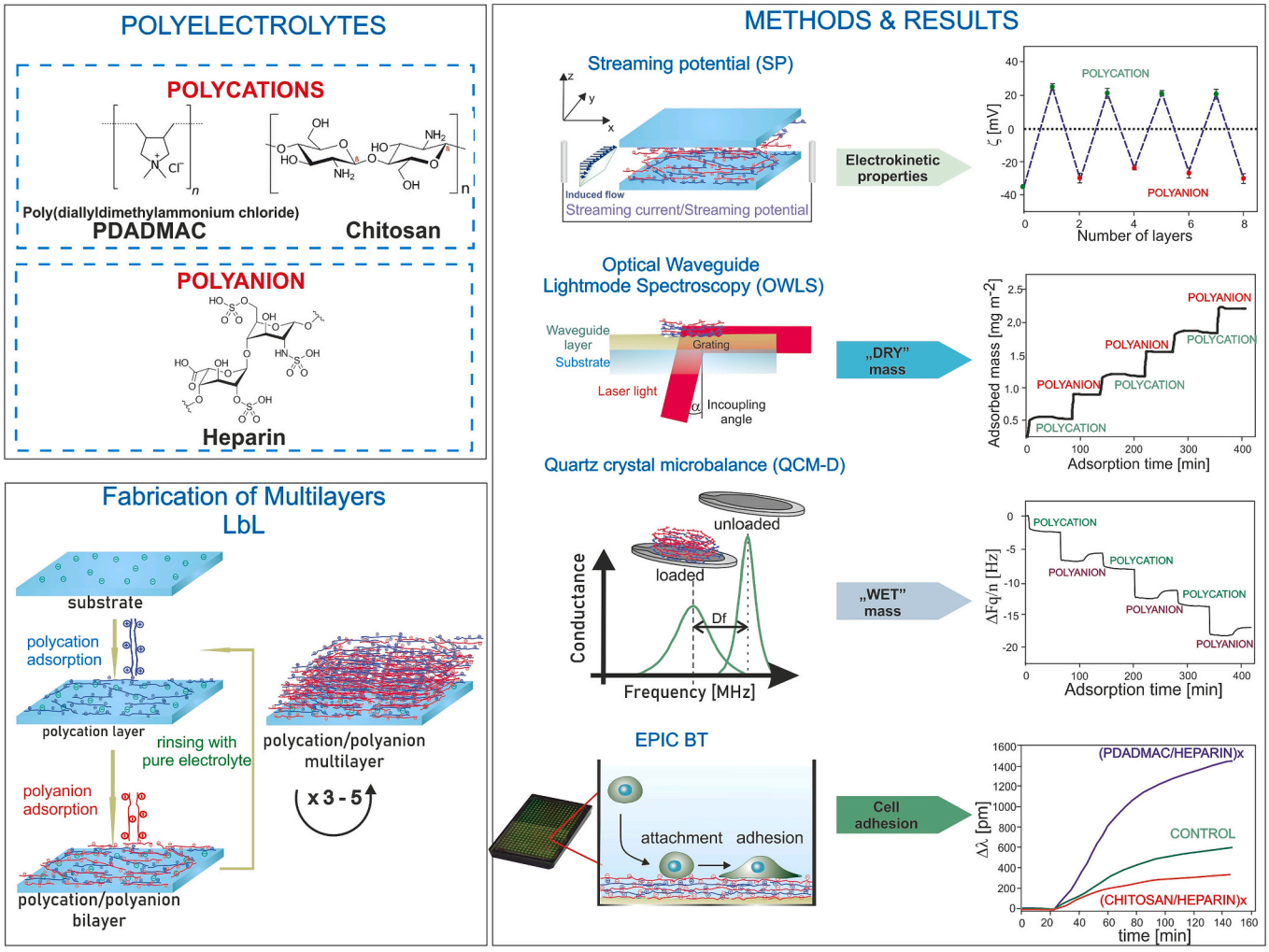

Fig. 1. Scheme representing the procedures used to prepare/investigate PDADMAC (or chitosan)/ heparin films.

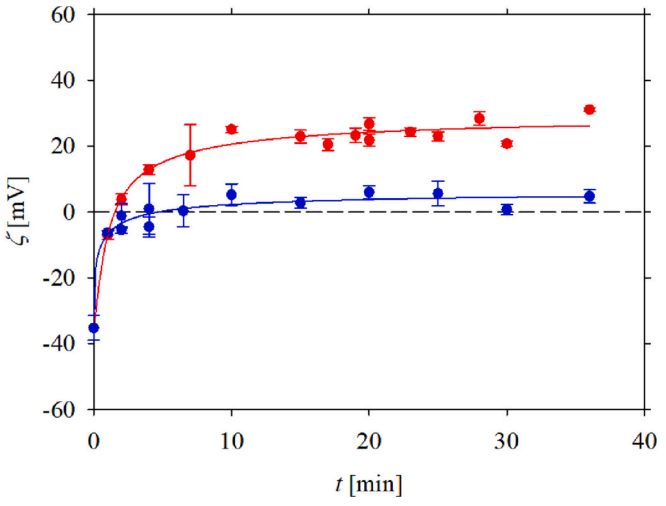

Fig. 2. Dependence of the zeta potential of silica (Si/SiO_2) (ζ) covered by PDADMAC (●) and chitosan (●) as a function of adsorption time (t). Points denote experimental results obtained for convection-controlled adsorption. The macrocation adsorption occurred at a flow rate of 0.01 ml s^{-1}. SPM was carried out in NaCl of I = 0.01 M and pH 5.8. Lines represent the fit of experimental data.

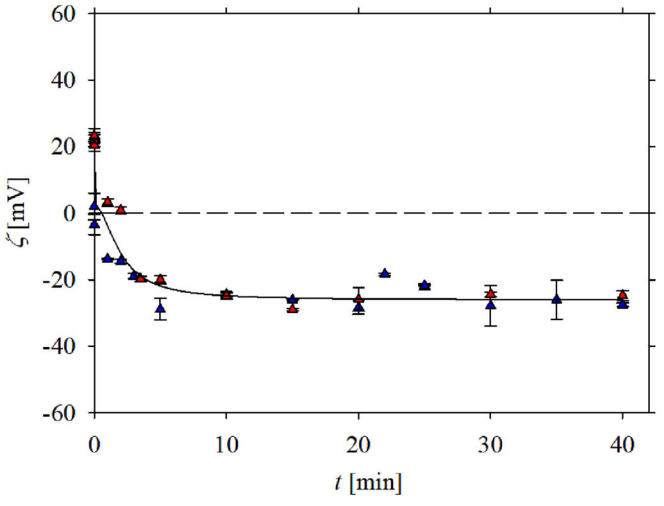

Fig. 3. Dependence of the zeta potential (ζ) of silica (Si/SiO_2) covered by PDADMAC (▲) and chitosan (▲) layer as a function of heparin adsorption time (t). Points denote experimental results obtained for convection-controlled adsorption of macroions at flow rate = 0.01 ml s^{-1} SPM were carried out in pure NaCl of I = 0.01 M and pH 5.8. A line represents the fit of experimental data.

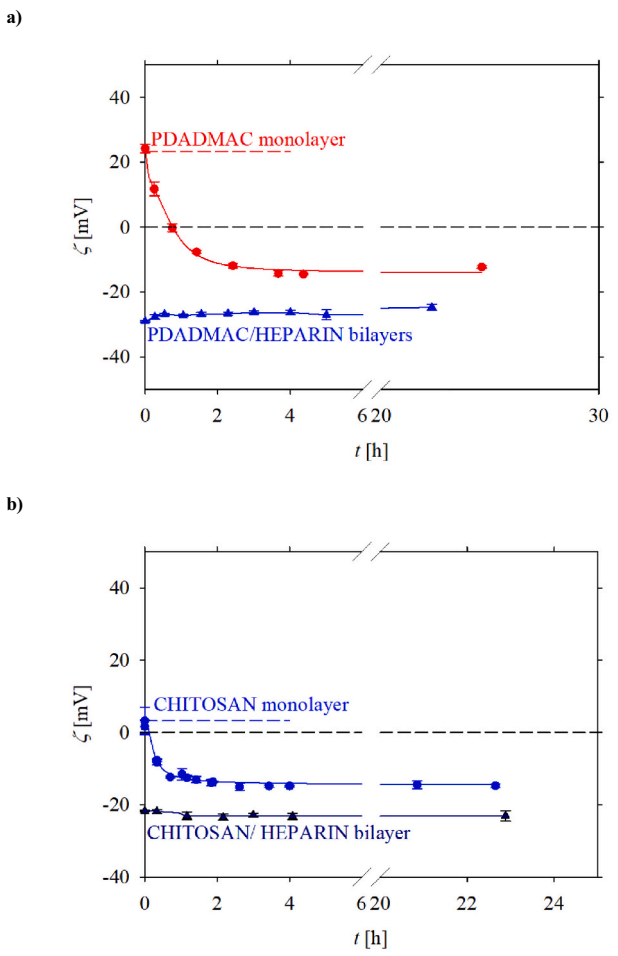

Fig. 4. Desorption kinetics of Part a) PDADMAC monolayer (●) and PDADMAC/heparin bilayer (▲); Part b) chitosan monolayer (●) and chitosan/heparin bilayer (▲) under flow conditions shown as the dependence of the apparent zeta potential (ζ) on the washing time (t). The points denote experimental results obtained from SPM for pH 5.8, 0.01 M NaCl. Lines represent the fit of experimental data.

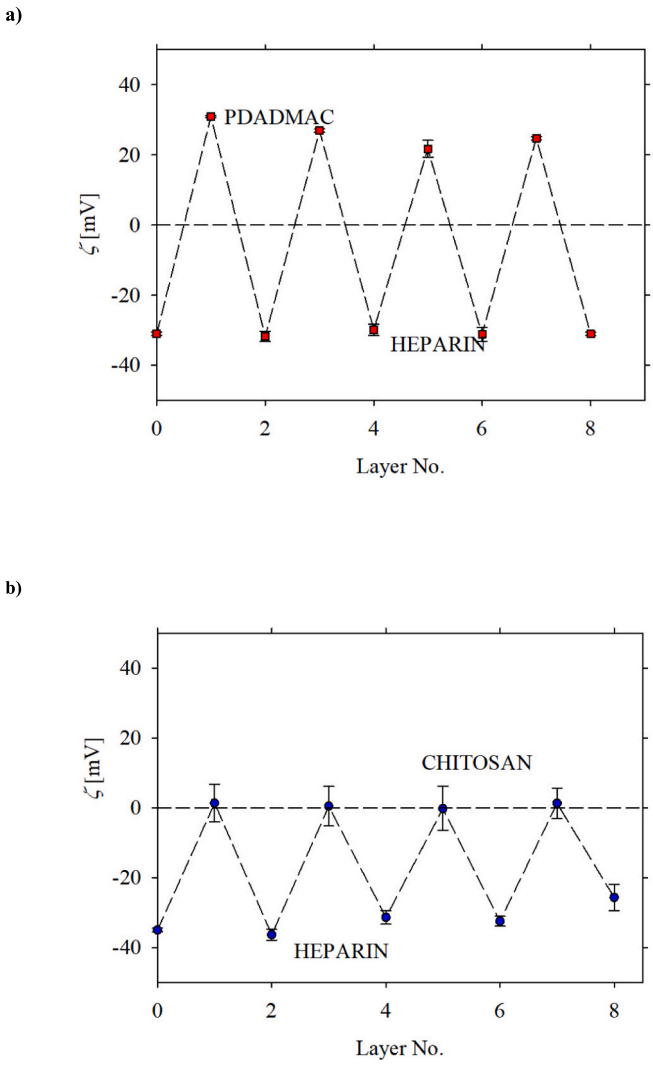

Fig. 5. The zeta potential of silica (ζ) as the function of the number of adsorbed layers (Layer No.) determined for a) PDADMAC/heparin b) chitosan/heparin multilayers. SPM were carried out in pure NaCl of $I = 0.01$ M and pH 5.8.

biosensors. One should be aware that also the other type of biomaterials, such as enzymes, antibodies can be used as biorecognition elements, whereas graphite, carbon paste, glassy carbon electrode, screen printed electrodes, and indium tin oxide are widely used as platform/sensor matrix [8] More examples of the biomaterials for the formation of effective biosensors can be found in the following books [9,10].

The ability of macroion films to promote cell adhesion depends on many factors, such as film mechanical properties, the internal structure of layers, the number of layers, hydration degree, charge density, or ending layer type. [11–15]

To fabricate the macroion films, the layer-by-layer (LbL) technique is applied. This method involves sequence-specific electrostatic interactions between macroion chains [16] for producing more complex structures with specific and controlled physicochemical properties [17]. Moreover, the LbL procedure is a universal technique as a large number of macroions, natural or synthetic, can be used to functionalize surfaces. This method enables development of bioactive macroion films for particular applications such as antibacterial surfaces, smart healing materials, tissue engineering, cell-supporting surfaces, coatings enhancing cellular behavior (e.g. the ones applied on biosensor surfaces) [9,10], and delivery systems for biologically relevant molecules [18–22].

Among a wide variety of macroions, used in LbL assembly processes, three of them have great potential in fundamental and practical research. Poly(diallyldimethylammonium chloride) (PDADMAC) is a synthetic, water-soluble polycation with a highly hydrophilic, positively charged quaternary ammonium group. It is fully positively charged throughout a broad pH range up to 11. If it is used in low concentrations, it demonstrates little-to-no cytotoxicity. In biotechnology, it is applied in the separation of proteins [23], biomolecule immobilization [24], and removal of bacteria from sludge [25].

In recent years, chitosan, being a natural polycation derived from chitin, has gained significant attention for its potential in tissue engineering applications [26]. Chitosan usually occurs as a copolymer of (1–4)-acetamido-2-deoxy-β-D-glucan (*N*-acetyl D-glucosamine) and (1–4)-2-amino-2- deoxy-β-D-glucan (D-glucosamine) units [27]. It is soluble in mildly acidic solutions. Due to its biodegradability and biocompatibility, it is extensively used in wound healing and tissue engineering. Chitosan is well known for its antimicrobial and antifungal properties, thus, it is used in biomedical scaffold formation. Chitosan effectively kills cancer cells by inducing their apoptosis [28]. Antimicrobial chitosan hydrogels and nanocomposites stimulate fibroblast attachment and proliferation without cellular toxicity [29].

Heparin is a glycosaminoglycan, also known as mucopolysaccharide. It naturally exists in ECM, where heparin molecules are bound to proteins forming proteoglycans. Accordingly, heparin regulates cell proliferation, cellular adhesion, matrix assembly, migration, immune

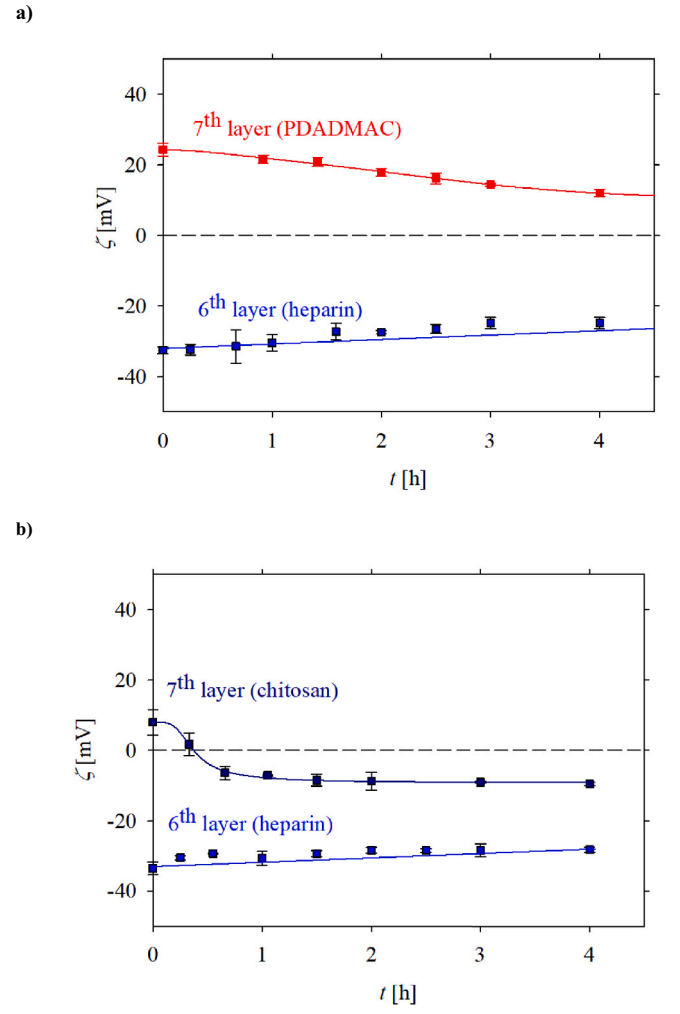

Fig. 6. Stabilities of a) the 6th layer terminated heparin (■) and 7th layer terminated PDADMAC (■); b) the 6th layer terminated heparin (■) and 7th layer terminated chitosan (■) on washing time (t). The points denote experimental results obtained from the SPM for pH 5.8, 0.01 M NaCl. Lines represent the fit of experimental data.

response, lipid metabolism, angiogenesis, and wound healing [30]. This glycosaminoglycan is well-known for its anticoagulant activity and has the highest negative charge density of all biological polyanions due to the presence of carboxyl and sulfonate groups within its chain [31,32]. Heparin modulates the biological activity of fibroblast growth factors and protects them from denaturation and enzymatic degradation [33–35].

The literature data suggest that the behavior of a murine osteoblast cell line, MC3T3-E1, is greatly affected by the surface on which it is grown. These cells easily adhere, proliferate, and mineralize on polymer films [36]. Indeed, when the MC3T3-E1 line was cultivated on the chitosan/collagen sponges, good attachment, growth, and differentiation enhancement of osteoblasts into the mature stage were observed [37,38]. These effects were explained by the presence of collagen, which is also a major component of ECM [37]. On the other hand, MC3T3-E1 cells growing at equivalent rates on polymer surfaces such as poly-(lactide-*co*-glycolide), and polycaprolactone as well as on unmodified glass were also reported [39]. Accordingly, the type of surface, mimicking ECM, allowing for efficient attachment and proliferation of the murine osteoblast cell line is still an open question.

Here we address this lack of knowledge and present comprehensive studies devoted to the in-depth physicochemical characterization of the (PDADMAC/heparin) and (chitosan/heparin) multilayers in defined ionic strength as well as pH and the impact of the heparin-based films on cell adhesion. These multilayers were built by sequential adsorption of macroions from solution with low bulk concentrations, i.e., 5 mg L^{-1}. The use of such low concentrations of macroions allowed for precise control of the structure of obtained layers. It is worth noticing that the films based on heparin, which naturally exists in ECM that mainly influence cell adhesion, have not been sufficiently characterized. Moreover, the adhesion of the murine preosteoblastic cell line on the heparin-based multilayers has not been determined yet.

The formation process, electrokinetic properties, and stability of the macroion-based materials were monitored by in situ streaming potential measurements (SPM), optical waveguide lightmode spectroscopy (OWLS), and quartz crystal microbalance with dissipation (QCM-D). Additionally, multilayer film topography and roughness were measured in liquid by atomic force microscopy (AFM).

Thoroughly characterized macroion layers were tested as supporting surfaces for preosteoblast cell adhesion. The impact of the macroion type forming the outer layer, the number of layers, and the charge of the outer layer on preosteoblastic cell adhesion were evaluated using a resonant waveguide grating (RWG) based optical biosensor. Evanescent wave-based optical biosensors detect refractive index changes near the sensor surface in a 100–200 nm thick sensing zone above the sensor surface, defined by the so-called evanescent field. The binding between the integrins in the cell membrane and the surface structures happen within the sensing zone, making these type of sensors ideal for monitoring cell surface adhesion events in real time [40–42]. Moreover, Sztilkovics et al. [42] have demonstrated that the recorded biosensor signal correlates with the directly measured single-cell adhesion force, but the throughput of the evanescent wave-based biosensors is significantly larger than that of the direct single-cell force measuring technologies. Digital holographic microscopy [43] was also employed to investigate long-term cellular behavior on the fabricated films in a label-free manner, mainly to prove long-term cell viability on the fabricated films.

We expect that the presented results allow for obtaining effective, based on heparin, surface coatings for favorable and controlled cellular adhesion that can be applied in advanced regenerative medicine in immunomodulation therapy, tissue engineering as well as the production of antimicrobial coatings for advanced medical devices.

2. Experimental section

2.1. Materials

Literature data do not clearly indicate which type of surface (soft, hard, homogeneous or heterogenous film) has a real impact on cell adhesion and proliferation. We decided to apply two various biocompatible macrocations, forming different types of layers, for further determination of cell adhesion. Poly(diallyldimethylammonium chloride) is strongly positively charged macrocation, whereas weakly positively charged chitosan is the only polysaccharide possessing a positive charge. Poly(diallyldimethylammonium chloride) -based films are homogenous, whereas gel-like structure is formed by chitosan layers. Heparin being a biocompatible, strongly negatively charged polysaccharide was applied as macroanion.

All materials used in the study were analytical grade and used without further purification. Poly(diallyldimethylammonium chloride), hereafter referred to as PDADMAC, having a molecular mass of 101 kg mol^{-1} (number averaged, M_n) and 160 kg mol^{-1} (weight averaged, M_w), was purchased from PSS Polymer Standards Service GmbH, Germany. Low molecular weight chitosan and heparin for physicochemical analysis were purchased from Merck. A thorough physicochemical analysis of the applied chitosan was performed in our previous paper [44]. It had an average molecular weight of 120 kg mol^{-1}, which was confirmed experimentally (viscosity method) and theoretically (the slender body hydrodynamics). The degree of deacetylation of chitosan was >75 %.

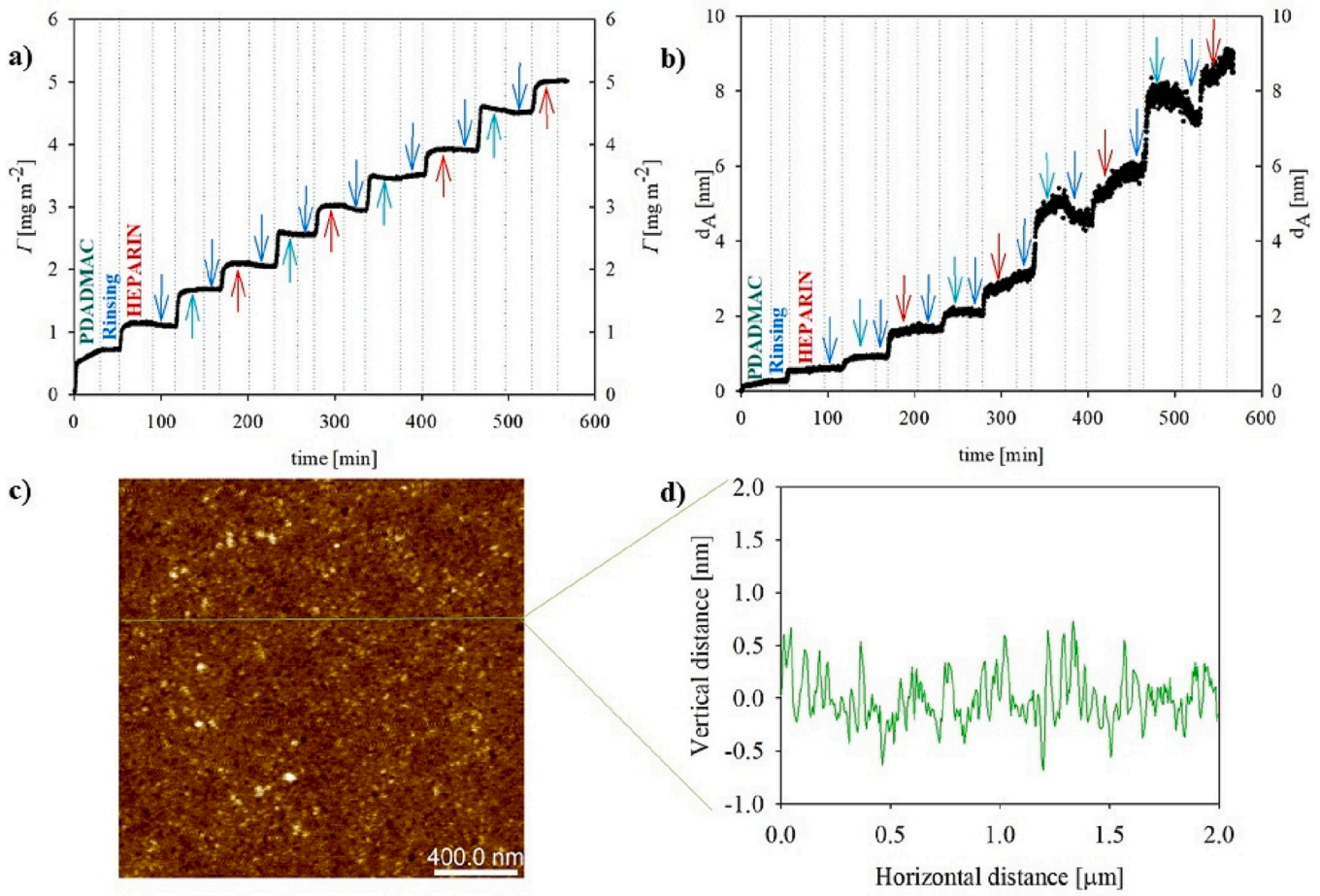

Fig. 7. Evolution of PDADMAC/heparin film monitored by OWLS. Adsorption was carried out for NaCl solution of $I = 0.01$ M, pH 5.8. a) adsorbed dry mass (Γ) as a function of time, b) thickness (d_A) of adsorbed film. c) AFM topography image of $(PDADMAC/heparin)_5$ film. d) cross-section profile of $(PDADMAC/heparin)_5$ film.

The influence of chitosan chains with different molecular weights on multilayer film formation and the corresponding changes in physicochemical properties of the films is a complex topic. Literature references do not explicitly identify these changes. For example, Bof et al. [45] suggest that the different molecular mass of chitosan has an impact on the physicochemical properties of the macroion film. However, no molecular weight effect was observed for the properties of the chitosan-based films formed in an aqueous solution by Tachaboonyakiat et al. [46]. On the other hand, Park et al. [47] reported that the tensile strength of the chitosan-based films increased significantly with the increase of its molecular mass while no significant difference was observed for the other properties of the macroion films. Water barrier property and tensile strength of chitosan films were improved along with an increased molecular mass of chitosan; however, film antibacterial capacities against *E. coli* and *L. innocua* were descended with increased molecular mass as was shown by Zhong et al. [48].

Phosphate buffer saline (PBS) and sodium chloride (NaCl) were also supplied by Sigma Aldrich. Sodium hydroxide (NaOH) and hydrochloric acid (HCl) were obtained from Avantor Performance Materials Poland S. A. (formerly POCH S.A., Gliwice, Poland).

PDADMAC and heparin powder were dissolved in a suitable buffer (NaCl, PBS) of desired pH (4 or 5.8) and ionic strength ($I = 0.01$ M) for obtaining the macroion solutions of a constant bulk concentration of 5 mg L^{-1} before each adsorption experiment. A suitable amount of chitosan powder was dissolved in 0.01 M HCl (pH 2.0) to obtain the solution of a bulk concentration of 100 mg L^{-1}. Then, the chitosan solution was diluted using 0.01 M NaCl to obtain the solution of a bulk concentration of 5 mg L^{-1} (pH 4.0).

The silicon wafers (plates) were the commercial product of Siegert Wafer GmbH (Germany) and were used as a model planar substrate for macroion adsorption experiments in streaming potential measurements. The silicon plates were cleaned by immersing them in piranha solution, which is a mixture (1:1 ratio) of 95 % sulfuric acid and 30 % hydrogen peroxide, for 30 min. After cleaning, the wafers were thoroughly washed with deionized water and immersed in 353 K water for 30 min. The wafers prepared in this way were stored in ultrapure water for no longer than 48 h.

The OWLS sensors (MicroVacuum Ltd., Hungary), made of glass support (refractive index $n_S = 1.52578$) coated with 170 nm $Si_{0.78}Ti_{0.22}O_2$ (refractive index $n_F = 1.8$) and an additional layer (10 nm) of pure SiO_2, were applied in optical waveguide lightmode spectroscopy (OWLS). OWLS sensors were cleaned with 3 % Hellmanex solution in an ultrasound bath for 30 min, then rinsed with ultrapure water at least 10 times, and dried with a gentle stream of nitrogen. In the next step of the cleaning procedure, sensors were placed in a UV cleaner for 15 min, rinsed with ultrapure water, and dried again with nitrogen. The sensors were immediately used thereafter.

The QCM- D sensors covered with SiO_2 (Qsense, Biolin Scientific) were cleaned with a 30- min old dissolved piranha solution (1:1:1 ratio of 95 % sulfuric acid, 30 % hydrogen peroxide, and distillate water) for 2 min. Subsequently, quartz crystals were rinsed with water (at least 10 times), boiled for 1 h, rinsed again, and dried with nitrogen. Sensors were used immediately after cleaning or stored in a desiccator before any experiment.

The osteoblastic cell line MC3T3-E1 (99072810, Merck KGaA, Darmstadt, Germany) was cultured in tissue culture polystyrene Petri

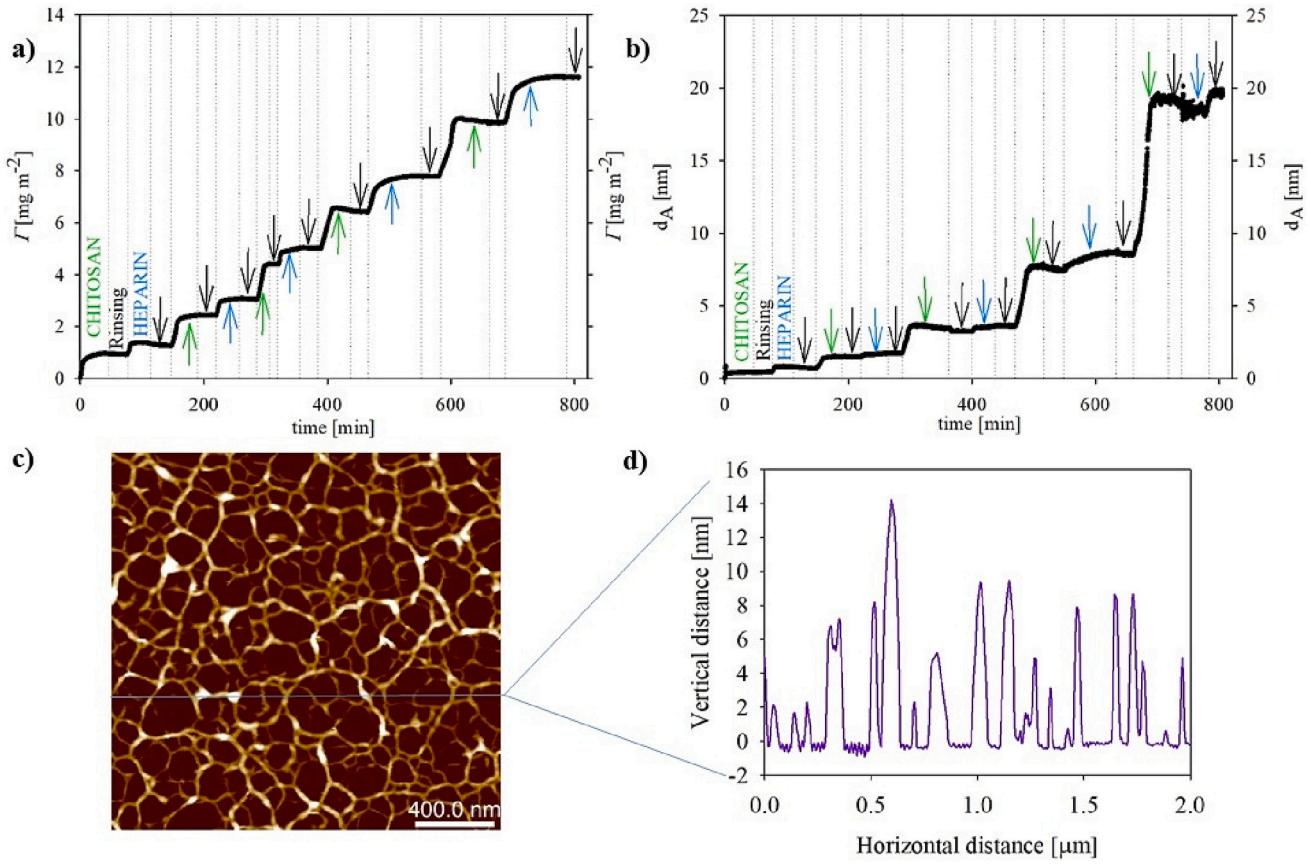

Fig. 8. Evolution of chitosan/heparin film monitored by OWLS. Adsorption was carried out for NaCl solution of $I = 0.01$ M, pH 5.8. a) adsorbed dry mass (Γ) as a function of time, b) thickness (d_A) of adsorbed film. c) AFM topography image of $(chitosan/heparin)_5$ film. d) cross-section profile of $(chitosan/heparin)_5$ film.

dishes (Greiner Bio-One International GmbH, Kremsmünster, Austria) in a humidified incubator (37 °C, 5 % CO_2). The cells were maintained in α-modified minimal essential medium (α-MEM, 22561021, Gibco), supplemented with 10 % fetal bovine serum (Biowest SAS, France), 0.002 M L-glutamine, 100 U ml^{-1} penicillin and 100 μg ml^{-1} streptomycin solution, and 0.25 μg ml^{-1} amphotericin B.

For the experiments, cells were detached from the Petri dish using a standard protocol with 0.05 % (*w/v*) trypsin and 0.02 % (w/v) EDTA solution. For the measurement with HoloMonitor (HM), cells were used in a complete growth medium. For the measurements with Epic BT, harvested cells were washed two times by centrifugation at 200 ×*g* for 5 min to remove the complete culture medium and the cell pellet was re-suspended in serum-free assay buffer, 0.02 M 4-(2-hydroxyethyl)-1-piperazineethanesulfonic acid (HEPES) in Hank's balanced salt solution (HBSS). Cells were then counted in a hemocytometer and diluted to a final cell density of 8000 cells per well.

2.2. Methods

2.2.1. Multilayer build-up and characterization

The preparation route of the macroion films is shown in Fig. 1 a. The film formation was conducted by alternative immersing of the substrates (silica wafers, OWLS, QCM-D sensors, or microplate wells) – in macrocation (PDADMAC or chitosan) and macroanion (heparin) solutions of bulk concentration of 5 mg L^{-1} for 20 min, followed by thorough rinsing with electrolyte after each adsorption step. The macroion layers were adsorbed alternately up to 10 layers (5 bilayers). One bilayer refers to one macroanionic layer on top of one macrocationic layer, and 0.5 layer refers to one macrocationic layer.

The measurements were repeated 3 times for each technique. In SPM method statistical error does not exceed 5 %. SPM and RWG graphs are plotted with standard deviation bars. However, it should be noted that the presentation of OWLS and QCM multiplot graphs containing error bars is practically impossible due to the discrepancy on the time axis. In the case of AFM imaging, the topology of the samples was determined from 5 to 10 AFM scans, each carried out over the areas of 2 × 2 $μm^2$, 5 × 5 $μm^2$, and 10 × 10 $μm^2$. All AFM topography maps were captured with a resolution of 384 × 384 pixels.

2.2.2. Streaming potential measurements (SPM)

Electrokinetic properties of the silica coated with macroion multilayers as well as multilayer stabilities were carried out by streaming potential measurements using the home-made apparatus described in detail in [49,50]. The streaming potential, ΔE_s, was measured in a two-electrode cell as a function of the hydrostatic pressure difference ΔP (see Fig. 1). Using the slope of this dependence, the zeta potential of the silica covered by the layers was calculated using the Smoluchowski equation [51].

The streaming potential method is capable of precisely determining the zeta potential changes with the particle coverage under in situ conditions. This creates a unique possibility to study particle adsorption and desorption kinetics in many configurations (charged particles/charged surfaces, neutral particles/charged surfaces, charged particles/neutral surfaces,).

The experimental procedure of evaluating the zeta potential consisted of measuring the zeta potential of a bare substrate (silica), then forming the desired number of macroion layers, and finally, without dismounting the cell, measuring the dependence of streaming potential on the hydrostatic pressure difference and determining the zeta potential.

The stability of the multilayers was also studied for longer times, reaching 24 h. After completing the desired number of layers, the zeta

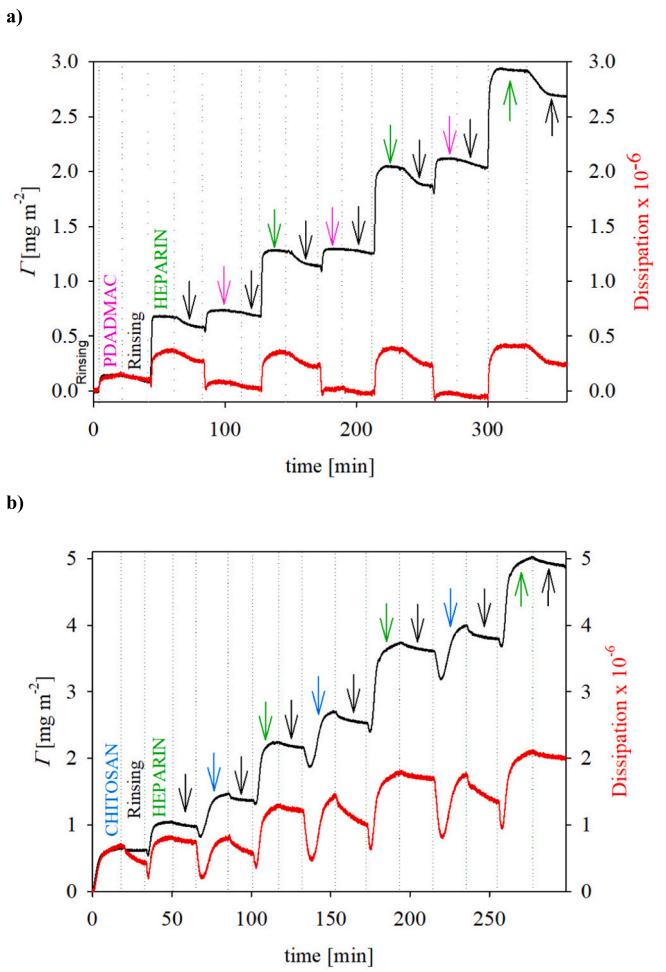

Fig. 9. Four bilayer formation monitored by QCM-D as a function of time: (a) PDADMAC/heparin film and (b) chitosan/heparin film. The adsorption process was carried out in NaCl solution of $I = 0.01$ M, pH 5.8 (PDADMAC/heparin), pH 4.0 (chitosan/heparin). Two QCM dependences were followed: mass uptake ($\Delta\Gamma$ [mg/m^2] calculated using Sauerbrey equation) vs time and ΔD (energy dissipation shift) vs time, respectively.

potential of multilayer conditioning in the pure electrolyte was established at specified time intervals.

Measurements were carried out for the initial bulk macroion concentration of 5 mg L^{-1}. The macroions were adsorbed inside the cell for a fixed period (0–40 min) under flow-controlled transport conditions (flow velocity, $V_{flow} = 0.01$ ml s^{-1}). pH and ionic strength of the solutions were 5.8 and 0.01 M, respectively.

2.2.3. Optical waveguide lightmode spectroscopy (OWLS)

The optical properties of the fabricated films were determined in situ by an OWLS 210 instrument (MicroVacuum Ltd., Budapest, Hungary). The setup is equipped with a laminar flow cell mounted on top of the silica-coated waveguide sensor (OW2400, Microvacuum Ltd.). A diffraction grating on the surface of the waveguide incouples a He—Ne laser beam at two well-defined incident angles for the zeroth order transverse electric (TE) and magnetic (TM) polarization modes [52,53]. Adsorption of molecules at the waveguide sensor surface alters the interfacial refractive index and, therefore, the incoupling resonant angles of the laser light are changed. This change is monitored in real-time with a time resolution of 3 s. From the measured changes in incoupling angles, the thickness and refractive index of the adsorbed layer can be calculated by assuming an optically uniform adsorbed layer [53]. The mass of adsorbed macroions per unit area Δm_{OWLS} is then calculated by Feijter's formula [54].

$$\Delta m_{OWLS} = d_A \frac{n_A - n_S}{(dn/dc)} \quad (1)$$

where d_A (cm) and n_A is the thickness and the refractive index of the adlayer, respectively, dn/dc is the refractive index increment of the macroion solutions, and n_S is the refractive index of the solutions.

OWLS is a powerful method capable of detecting structural changes of adlayer components. Both layer adsorption kinetic and nanostructure can be analyzed by this technique. In contrast to QCM-D, the OWLS technique provides the dry mass per unit area of adsorbed molecules [53]. Additionally, OWLS offers a detection limit of <1 ng cm^{-2} and the independent measurement of n_A and d_A.

A standard procedure in situ OWLS experiment started with the flow of pure electrolyte solution to condition the surface and to achieve a stable baseline ($\Delta m < 15$ ng cm^{-2} per 1 h). As silica covered sensor is negatively charged [55], the first macroion layer was formed by supplying a solution of positively charged macroion (PDADMAC or chitosan) over the sensor surface, which resulted in a signal shift. Upon adsorption onto the sensor's surface, the effective refractive index shifts to higher values, allowing for in situ monitoring of the kinetics of adsorption processes. After a rinsing step with electrolyte solution, which was applied to remove the loosely bound molecules from the surface, the negatively charged heparin solution was added and the kinetics of heparin adsorption was monitored. The experiment ended with a rinsing phase. After achieving a stable final signal the whole procedure was repeated 3 to 5 times to obtain the desired number of layers. As can be seen in Fig. 1 c alternatively supplied macroions produce an increase in the OWLS mass. This shows that multilayers composed of PDADMAC/heparin and chitosan/heparin are being formed on the surface.

2.2.4. Quartz crystal microbalance with dissipation (QCM-D)

The formation of PDADMAC/heparin and chitosan/heparin multilayers on silica-coated QCM sensors was determined by a Q-Sense E1 system (QSense, Gothenburg, Sweden) following the standard procedure described in Ref. [56]. QSense setup allows for data acquisition up to 300 datapoints per second and therefore exceptional mass sensitivity (0.5 ng/cm^2).

A stable baseline of the electrolyte (NaCl) at a fixed ionic strength of 0.01 M and pH value (5.8 for PDADMAC/heparin and 4.0 for chitosan/heparin films, respectively) was acquired in the QCM-D cell for a defined electrolyte flow (1.33×10^{-3} cm^3 s^{-1}). Subsequently, the solution of PDADMAC or chitosan with the bulk concentration of 5 mg L^{-1} was introduced into the cell. Adsorption of positively charged macroion on the negatively charged sensor was monitored in situ. After reaching a plateau by two QCM parameters dependences (frequency shift ΔFq and energy dissipation shift ΔD as a function of time), the attached layer was flushed by the pure electrolyte, and the desorption process of loosely bound molecules was followed. Thereafter, a 5 mg L^{-1} solution of heparin was introduced into the cell. The adsorption of the negatively charged layer was carried out in the same way as the formation of the positively charged layer. Each step of the experiment (layer formation and rinsing of adsorbed layer) was carried out until the plateau values of ΔFq vs. time and ΔD vs. time were obtained, i.e., for 20–30 min. The whole procedure was repeated until the assembly of 5 bilayers (PDADMAC/heparin or chitosan/ heparin) was acquired. The measurements were completed at 298 K.

2.2.5. Atomic force microscopy

The topography of tested multilayers was investigated using atomic force microscopy (AFM, Dimension ICON, Bruker, Santa Barbara, CA, USA) working in the PeakForce Tapping® (PFT) and QNM® modes. The topography measurements were performed in water under low loading forces (typically 2 nN) using ScanAsyst-fluid probes to exclude sample damage and limit the compression. The spring constant of the probe was

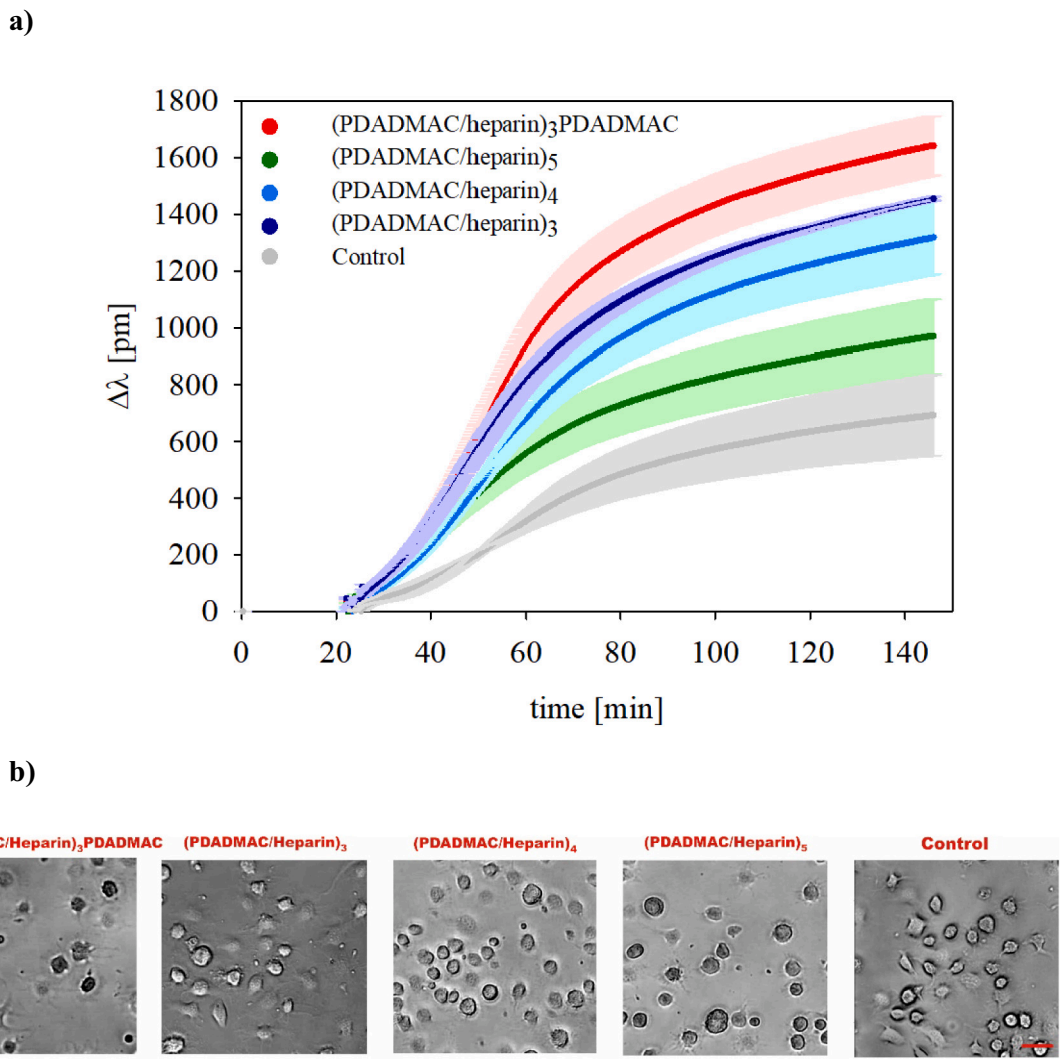

Fig. 10. Part a) Kinetics of adhesion of preosteoblast cells on PDADMAC/heparin films. The data were obtained in triplicates ($n = 3$)) ± SD. Part b) Phase contrast images of preosteoblast cells on the PDADMAC/heparin films. Scale bars represent 50 μm.

calibrated by the thermal-noise method. The deflection sensitivity of the optical beam-detection system was calibrated on a freshly cleaned mica surface. The roughness parameters of (PDADMAC/heparin) and (chitosan/heparin) layers were determined from 2 × 2 μm topography maps (total resolution of 384 × 384 pixels) using NanoScope Analysis software.

2.2.6. Resonant waveguide grating (RWG) optical biosensor

To investigate the impact of the macroion type, the number of layers and the charge of the outer layer on the cell adhesion the resonant waveguide grating (RWG) based Epic BT instrument (Corning Incorporated, Corning, NY, USA) was applied. The measurements were performed in 384-well uncoated Epic cell assay microplates (#5040, Corning Incorporated, Corning, NY, USA) that bottom consists of a Nb_2O_5 layer supported by a glass substrate in each well. The grating structure embedded in the waveguide allows to incouple one wavelength (the resonant wavelength, λ) from the broadband light (825–840 nm) illuminating the sensors. The evanescent field is formed after the excitation of the waveguide at the resonant wavelength. The penetration depth of this field is around 150 nm and its intensity decays exponentially from the surface of the sensor. After some short, micrometer scale, propagation in the waveguide the resonant light is outcoupled from the waveguide by the same grating structure used for incoupling. The outcoupled resonant wavelength is detected by the instrument with a 0.25 pm resolution. The resonant wavelength where the in- and outcoupling happens depends on the refractive index of the material above the sensor, inside the evanescent sensing zone. When the refractive index of the material above the sensor surface changes, the resonant wavelength is altered leading to a new value ($\lambda' \neq \lambda$). (Of note, living cells have a larger refractive index than that of the aqueous solutions, therefore they increase the local refractive index in the sensing zone during their surface adhesion process. The cell adhesion process leads to an increase in the resonant wavelength.) The instrument's camera detects the reflected wavelength of light coming out of the sensor every 3 s. The biosensor measures the shift of resonant wavelength ($\Delta\lambda = \lambda'$-λ) in each well over time. It should be underlined that the sensor possesses a low limit of detection, which is 0.078 ng cm^{-2} [40,57].

At the beginning of the measurements, the buffer baseline was recorded in physiological conditions (0.15 M PBS buffer, pH 7.4) for 10 min, then the macrocation solution of concentration of 5 mg L^{-1} was pipetted into the wells where it was stored for 30 min. In the next step, the adsorbed macrocation layer was washed three times with NaCl solution. Then, the macroanion was pipetted into the wells, in the same way as the macrocation. After 30 min of incubation, the wells were again washed three times with the NaCl buffer. These steps were repeated five times, which resulted in five bilayer formations. Subsequently, all wells were rinsed three times with 0.02 M HEPES HBSS buffer, and baselines were recorded in the assay buffer for 10 min. Meanwhile, the cells were

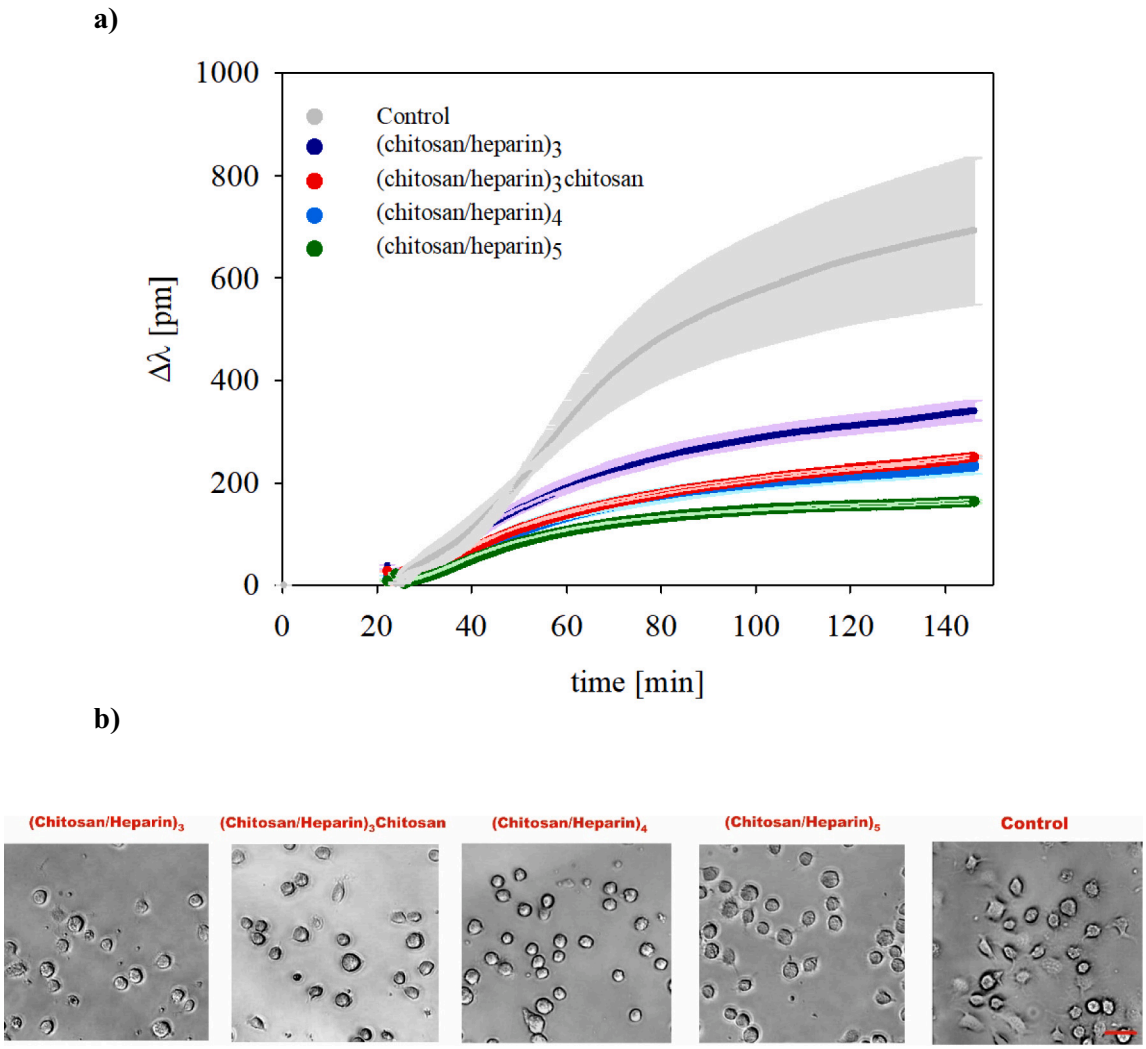

Fig. 11. a) Kinetic of adhesion of preosteoblast cells on the surface coated with (chitosan/heparin) films. The data were obtained in triplicates ($n = 3$) ± SD. b) The phase contrast images of preosteoblast cells on the chitosan/heparin films. Scale bars represent 50 μm.

prepared as described above in the Material section. 25 μl of cell suspension, containing 8000 cells, was added to the sensor wells. Biosensor signals were recorded for 4 h at room temperature. All measurements were replicated three times.

2.2.7. Digital holographic microscopy

Morphological parameters of preosteoblastic cells on different coatings were studied using the label-free time-lapse cytometer HoloMonitor M4 (Phase Holographic Imaging AB, Lund, Sweden). Macroion multilayers were prepared in 96-well Sarstedt tissue culture plates in triplicates. Cells were seeded at a density of 2500 cells per well in 200 μl complete growth medium, and wells were covered with HoloLid. Three regions of interest were assigned in each well automatically, and images were taken every hour for 48 h inside a humidified incubator. HoloMonitor images were evaluated by HStudio (Phase Holographic Imaging AB, Lund, Sweden) and data were analyzed in GraphPad Prism 8.0 (GraphPad Software, La Jolla, CA, USA) [58–62].

3. Results and discussion

3.1. Streaming potential measurements (SPM)

Streaming potential measurements (SPM) working under in situ conditions provide essential information regarding the electrokinetic state of macroion-covered substrates.

Primary experimental results on the dependence of the zeta potential of silica on macrocation adsorption time are presented in Fig. 2.

One can observe that stationary zeta potential values were obtained after 10 min of adsorption from 5 mg L^{-1} of PDADMAC and chitosan. However, the maximum zeta potential value of silica covered by PDADMAC was much higher than that obtained for chitosan-coated silica. Accordingly, one can state that only PDADMAC forms a monolayer on silica, whereas chitosan adsorbs on the surface in small amounts, without forming a monolayer in these conditions.

Similar dependences and final zeta potentials were obtained for PDADMAC monolayers adsorbed on silica and formed by adsorption from solutions of the same macroion concentration and ionic strength but various pHs, i.e., 4.0 and 7.4. Results were presented in Fig. S1 in Supplementary Materials.

In the next step, the silica-coated with either preadsorbed PDADMAC or chitosan layer was applied as a substrate for evaluating the adsorption kinetics of heparin. PDADMAC and chitosan were adsorbed for 20 min from the bulk concentration of 5 mg L^{-1}.

As can be seen in Fig. 3, the heparin adsorption kinetics is independent of the type and final charge of preadsorbed monolayers. Similarly to the first monolayer, the stationary value of −25 mV is attained after 10 min. of the heparin adsorption.

SPM can be also exploited for determining the stability of every layer

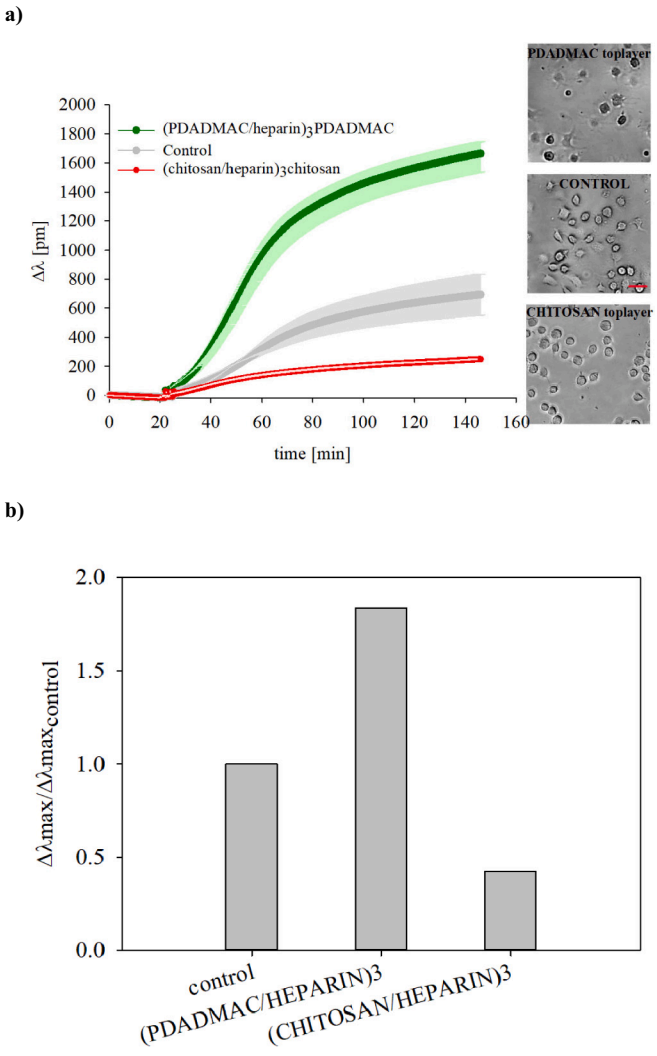

Fig. 12. a) Kinetic of preosteoblast cells attached to $(PDADMAC/heparin)_3$-PDADMAC (—) and $(chitosan/heparin)_3$chitosan (—) films, respectively. The grey curve represents data for the control sample (uncovered surface). The data was obtained in triplicates (n = 3) ± SD. The inset shows phase contrast images of preosteoblast cells on the biosensor surfaces covered by macroion films. Scale bars represent 50 μm. b) Normalized maximum biosensor response $\Delta\lambda_{max}/\Delta\lambda max_{control}$ as a function of the macroion multilayers composition. Scale bars represent 50 μm.

against rinsing [63].

In Fig. 4 a-b one can observe the consecutive changes in the zeta potential of silica covered by the monolayers with flushing time. Initial values of the zeta potentials of PDADMAC and chitosan monolayers systematically decrease from 28 mV and 5 mV, respectively, to a stable final value of −15 mV (after 24 h) (see Fig. 4a-b).

Contrary to the monolayers, the PDADMAC/heparin and chitosan/heparin bilayers remain stable for prolongated washing time (see Fig. 4 a-b, blue and dark blue triangles). The obtained results suggest that the heparin, due to its high negative charge, effectively immobilizes the macroion chains leading to the formation of stable bilayers. It is worth underlying that immobilized heparin also effectively binds proteins as was shown in Refs. [64, 65].

The procedure of layer-by-layer adsorption of PDADMAC (or chitosan) and heparin on silica substrate was continued. By plotting the zeta potential of the consecutive layer against the layer number, one obtains a zig-zag pattern, see Fig. 5 a-b.

Adsorption of the consecutive layers leads to zeta potential inversion, and these changes become quite periodic. The zeta potential of the layers, determined for the ionic strength of 0.01 M and pH 5.8, attained 26 mV for PDADMAC, 1 mV for chitosan, and − 31 mV for heparin, respectively. The presented results indicated that the zeta potential of consecutive heparin layers was constant and independent of the charge of the preadsorbed layer (PDADMAC or chitosan). It is worth mentioning that at pH 5.8 and under undefined ionic strength, the same value of zeta potential (−31 mV) of glass covered by four (chitosan/heparin) bilayers, where heparin formed the outer layer, was determined by Zhou et al. [66]

Almost identical values of zeta potentials of PDADMAC layers were reported for PDADMAC/bovine serum albumin multilayer-covered silica nanoparticles [67].

Inspecting Fig. 5b, one can observe that the zeta potentials of successive chitosan-terminated layers are significantly lower than the zeta potentials of PDADMAC-terminated layers. This indicates that chitosan/heparin can form rather heterogeneous structures than homogeneous films in these conditions.

The results shown in Fig. 5 indicate that the SPM are useful for efficiently characterizing in situ electrokinetic properties of macroion multilayers.

Additionally, SPM were exploited for determining the stability of macroion films against washing. The obtained results are presented in Fig. 6a-b.

Upon adsorbing the desired number of macroion layers, the cell channel was flushed with electrolyte (0.01 M at pH 5.8). The streaming potential was measured at defined intervals. As can be seen in Fig. 6, the changes in zeta potentials of the 6th layers, terminated with heparin, were practically negligible. On the other hand, the zeta potentials of the 7th layers (terminated either with PDADMAC or chitosan) successively decreased with time. However, in both cases (multi-layered assembly with either PDADMAC or chitosan as the outermost layer) the 7th layers were more stable against washing than the first ones (see Fig. 4).

It should be pointed out that it is not possible, without additional measurements, to unequivocally attribute the differences in layer stability to washing. However, one can suggest that the higher resistance against the washing of heparin may be associated with the possible cross-linking properties of heparin, or stronger ionic interaction of heparin being a stronger macroion than chitosan.

3.1.1. OWLS measurements

Macroion multilayer formation on SiO_2 coated sensors was monitored in situ using optical waveguide lightmode spectroscopy (OWLS). It allows one to determine the total optical mass of each adsorbed macroion layer and its stabilities. As the silica-coated sensor is negatively charged under applied experimental conditions the first layer was formed by the adsorption of positively charged PDADMAC or chitosan. After the rinsing step with pure electrolyte, the negatively charged heparin was adsorbed. The adsorption of oppositely charged macroions was continued until the film composed of 5 bilayers was created.

The dependencies of the dry mass of successively adsorbed $(PDADMAC/heparin)_5$ and $(chitosan/heparin)_5$ layers as the function of time are shown in Figs. 7 and 8, respectively.

At first inspection, it can be observed that the mass of adsorbed PDADMAC/heparin layers increases with the adsorption steps (Fig. 7a). Furthermore, the sequential adsorption of strong, oppositely charged macroions (PDADMAC and heparin) leads to the formation of stable films, which are resistant to rinsing. As can be seen in Fig. 7a an adsorbed mass increases linearly with the adsorption steps. One should notice that in each step the same mass equals ~1.1 mg m^{-2} per one bilayer is adsorbed. The PDADMAC/heparin film thickness increases during the adsorption of the subsequent layers in a linear fashion reaching a value of 8 nm for 10-layer film (see Fig. 7b).

An interesting result concerning the changes in the surface properties of the macroion films caused by graphene oxide incorporation were reported by Andreeva et al. [68]. The authors found that the type of

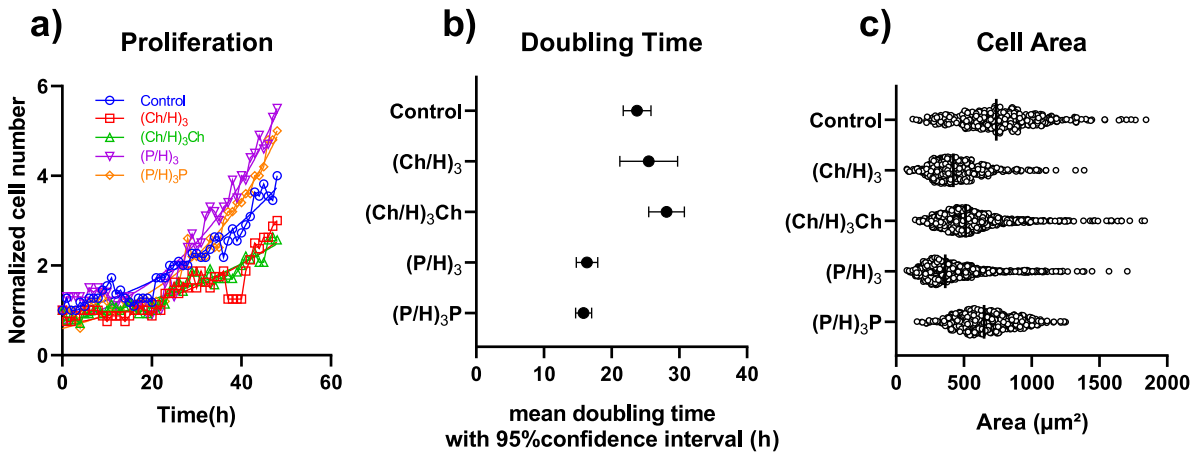

Fig. 13. Preosteblast parameters determined by digital holographic microscopy. a) Proliferation of the preosteoblast cells normalized to the initial cell number on each multilayer fitted with the exponential growth model. b) Mean doubling time of preosteoblast cell areas on the various multilayers as estimated by the fitted exponential growth model coefficient. c) Distribution of the cells on each surface type throughout the 48-h measurement, the vertical bar represents the median. $(Ch/H)_3$ - $(chitosan/heparin)_3$, $(Ch/H)_3Ch$ - $(chitosan/heparin)_3chitosan$, $(P/H)_3$ - $(PDADMAC/heparin)_3$, $(P/H)_3P$ - $(PDADMAC/heparin)_3PDADMAC$.

applied macroions, either strong synthetic or weak natural, had a strong impact on the thickness of the adsorbed macroion films. Accordingly, the growth mechanism of the macroion films can be modulated by choosing the suitable types of macroions.

The AFM image of PDADMAC/heparin layers (Fig. 7c) showed fairly homogenous morphology of the obtained films, which is also visible in the generated height profile (Fig. 7d) and confirmed by a low value of the average roughness (R_a = 0.3 nm) (Fig. 7c). Strong interactions between PDADMAC and heparin, which are both strong macroions, suggest that obtained films have a rather rigid structure.

The dependence of adsorbed mass on the number of layers of the chitosan/heparin system exhibits a nonlinear growth (Fig. 8a). During the adsorption of 6 layers, the mass increment per adsorbed macroion pair is of a similar amplitude reaching ~1.4 mg m^{-2}. As the adsorption process continues the mass growth becomes higher and reaches a value of ~2.1 mg m^{-2}. This film is thicker than the PDADMAC/heparin one with a thickness equal to ~20 nm for the film made of 10 layers (see Fig. 8b).

The AFM images of $(chitosan/heparin)_5$ film (Fig. 8 Part c) revealed a heterogenous, nanofibril/spongy-like structure with uncovered regions of silicon. The height of the nanofibrils reaches 10–15 nm (Fig. 8 Part d). As a result, the obtained film exhibits substantially larger average roughness R_a (3.1 nm) compared to $(PDADMAC/heparin)_5$ sample. It is suggested that the formation of fibrilar chitosan/heparin structures is responsible for an exponential buildup of the film. The observed exponential growth of the film can be also explained by the diffusion of at least one type of macroion chains into and out of an assembled film, as was shown by Boulmedais et al. for poly-L-lysine/heparin multilayers [69]. It should be noticed that OWLS and AFM results are well correlated with the ones determined from SPM, where the zeta potentials of subsequent chitosan/heparin layers were much lower than PDADMAC/heparin layers.

To confirm the various viscoelastic properties of PDADMAC/heparin and chitosan/heparin films, the gravimetric method (QCM-D) was applied.

3.1.2. QCM-D measurements

QCM-D was employed to study in situ the formation and stability of wet films composed of four bilayers: $(PDADMAC/heparin)_4$ (Fig. 9a) and $(chitosan/heparin)_4$ (Fig. 9b). The multilayers were adsorbed on SiO_2 covered quartz sensor and their adsorption process was monitored via a shift of two main QCM parameters as a function of time: ΔFq (frequency shift- representing mass uptake $\Delta\Gamma$ of the sensor during adsorption via Sauerbrey eq. [56]) and ΔD (dissipation shift- following the viscoelastic properties variations of the adsorbate during an experiment).

QCM data confirm the formation of 4 bilayers for both macroion systems. $(PDADMAC/heparin)_4$ consists of stable (rinsed) PDADMAC layers with an average mass of 0.2 mg m^{-2} covered with a stable heparin layer of 0.5 mg m^{-2} (Fig. 9 Part a – black curve), reaching the wet mass of 2.6 mg m^{-2} of 4 bilayers. On the other hand, the dissipation shift (Fig. 9 Part a – red curve) does not increase with the mass uptake, reaching a maximum value of 0.25 [dissipation unit] by the formation of the fourth bilayer, suggesting that the system $(PDADMAC/heparin)_4$ remains rigid. One should notice that the same conclusions could be drawn based on the results obtained from the OWLS measurements.

The second multi-layered system $(chitosan/heparin)_4$ is thicker and softer (Fig. 9 Part b) than the previous assembly. The average mass uptake by adsorption of chitosan film is 0.6 mg m^{-2} (Fig. 9 Part b-black curve). Heparin adsorbed on each chitosan layer with increasing mass (1st bilayer- 0.36, 2nd-0.84, 3rd-1.22, and 4th −1.21 mg m^{-2}), reaching wet mass uptake of almost 5 mg m^{-2} of the whole system. Dissipation shift increased with the deposition of each layer up to the value of 2.0 [dissipation unit], implying significant viscoelastic properties of the adsorbate (Fig. 9 Part b- red curve). The observed negative spikes of $\Delta\Gamma$ and ΔD at the point of chitosan solution injection can be attributed to structural deformation of the adsorbate and changes in the solution density, followed by typical mass uptake signal $\Delta\Gamma$ and ΔD increase [70].

3.1.3. RWG optical biosensor measurements

Kinetics of preosteoblast cell adhesion was monitored using a 384-well Corning Epic biosensor microplate. During the experiments always 8000 cells were added to each well. The delta lambda axis (Δλ) shows the wavelength shift from the baseline value measured by the biosensor. The greater wavelength shift means a greater change in refractive index value, i.e. the greater degree of cell adhesion. Both the contact area and the contact strength increase during the adhesion process, increasing the local refractive index inside the sensing zone, which leads to an increased biosensor signal (Δλ).

Microscopic images were not taken on the entire well surface, but only of small local places at each condition. There is the same number of cells in each well, but the distribution of cells in the images may differ in specific locations. These images provide visual information about the morphology and spreading conditions of the cells on each surface. The typical adhesion kinetics of preosteoblasts to PDADMAC/heparin and chitosan/heparin films are presented in Figs. 10 and 11, respectively.

Cell adhesion is autocatalytic, and a self-induced dynamic process, which results in the cell contact area enhancement on the surface by the

direct interaction between the integrins and surface ligands. During the cell spreading process the cell contact area increase on the sensor surface over time, and the biosensor record a sigmoidal kinetic signal (see Fig. 1 Methods and Results). The sigmoidal curve usually applies to describe active, living processes or in some special cases in chemistry stands for autocatalytic processes, too [57,71,72]. The adsorption of the non-living species results in a kinetic curve with a monotonically decreasing slope [4,57]. In an earlier publication, we have shown that the sigmoid character of the adhesion kinetic curves correlates well with the viability of the cells, dying cells lose their capability to respond actively to external stimuli and thus lose their sigmoidal adhesion character [57].

As can be observed a sigmoid-like response, a typical characteristic of active, living processes, was obtained for each PDADMAC/heparin film. PDADMAC/heparin films enhanced preosteoblast cell adhesion compared to cell adhesion to the uncoated sensors (see a grey curve in Fig. 10a). The adherence of cells decreases with the number of PDADMAC/heparin bilayers. The highest wavelength shift is obtained for $(PDADMAC/heparin)_3$PDADMAC film – seven layers system ended with a positively charged macroion layer. This indicates that the strongest adhesion of the cells to film is observed for PDADMAC terminated layers (see the red curve in Fig. 10a). It is known from the literature, that cells possessing a negative surface charge [73] strongly interact with the positively charged surfaces [74]. The microscopy images of cells on the biosensor surface taken directly after the measurements confirm cell adhesion to macroion multilayers.

Heparin, being a member of the sulfated glycosaminoglycans (GAG) family, may enhance cell adhesion by interacting with cell surface receptors. However, PDADMAC also contributes to cell adhesion. We suggest that the presence of quaternary cations on the PDADMAC chains can affect the stronger adhesion of preosteoblast cells by increasing the electrostatic interactions between strongly positively charged PDADMAC and negatively charged cell membranes.

The additional kinetic curve of cell adhesion on the PDADMAC monolayer was obtained. Results are presented in Fig. S2 in Supplementary Materials.

Analyzing the biosensor signals (Fig. 11a) obtained for cell adhesion to chitosan/heparin films, significant inhibition of cell adhesion can be observed. Similarly to PDADMAC/heparin system the number of chitosan/heparin layers influences preosteoblast cell adhesion, but in contrary to film with PDADMAC outmost layer, see Fig. 11a, cells adhered less on film terminated chitosan than at heparin ended one. We postulate that weaker electrostatic interactions are present between chitosan and heparin in chitosan/heparin multilayers. Hence, higher hydration and reduced stiffness can lead to decreased cell adhesion. Richert et al. also hypothesize that stiff films can enhance the cell adhesion process. They found that myoblasts cells adhered less and spread very low on soft poly-L-lysine/ hyaluronic acid films as compared to stiff poly-L-lysine/hyaluronic acid crosslinked ones [75]. Additionally, the possible diffusion of heparin into multilayers, as implied by Boulmedais et al. [69] can affect the conformation of heparin molecules and prevent interactions with cell receptors.

The obtained results indicate that the cell adhesion is also sensitive to surface charge. In Fig. 12 Part b the normalized maximum biosensor response ($\Delta\lambda max/\Delta\lambda max_{control}$) as the function of macroion multilayers clearly indicates charge-dependent reduction on cell adhesion. As can be observed (chitosan/heparin) films with chitosan terminated layer, exhibiting almost neutral net charge (see Fig. 5), inhibited cells adhesion. Cells adhered less on this barely charged film as compared to highly positively charged PDADMAC ended $(PDADMAC/heparin)_3$-PDADMAC film.

3.1.4. Digital holographic microscopy

To assess the capability of the multilayers to support adherent cell culture, preosteoblast cells were monitored for 48 h with digital holographic microscopy. The proliferation of preosteoblast cells on the various multilayers was compared to that on the control tissue culture surface. By tracking cells within a defined area, we estimated the doubling rate of proliferation by fitting an exponential growth model to the normalized cell number detected within the area (Fig. 13a). Doubling time was reduced by approximately 30 % on PDADMAC-containing multilayers compared to the control. In contrast, a slight increase was observed on the chitosan-containing surfaces in comparison to the control surfaces, with the highest increase of approximately 10 % was observed on $(chitosan/heparin)_3$-chitosan (see Fig. 13b). This can, in part, be explained by the decrease in cell spreading observed on the chitosan-containing surfaces, as indicated by a lower average cell area (see Fig. 13c). This finding is consistent with the results obtained from the RWG biosensor. Interestingly, on PDADMAC/heparin multilayers the presence of PDADMAC as the top layer led to larger cell areas compared to when heparin was the top layer. However, this difference did not have an impact on the proliferation rate of the cells (Fig. 13c). Representative images of results obtained with the digital holographic microscopy are presented as Fig. S3 in Supplementary Materials. It is important to note that the observed behavior on the PDADMAC-containing layers (reduced doubling time and decreased cell area) could potentially be attributed to the limited vertical resolution of the Holomonitor instrument, which may have resulted in undetected cell areas [43].

4. Conclusions

The physicochemical properties of PDADMAC/heparin and chitosan/heparin films and their impact on preosteoblast cell adhesion and spreading were successfully evaluated by various experimental methods such as SPM, OWLS, AFM, QCM-D, RWG- based optical biosensor and digital holographic microscopy. The applied techniques provided important information concerning the formation of effective coatings for favorable cell adhesion.

Upon adsorption of the positively charged macrocations (PDADMAC or chitosan), the zeta potential of silica changed its sign. Further adsorption of consecutive PDADMAC, chitosan, or heparin layers led to periodic oscillations of zeta potential. The macroion multilayer terminated by heparin was significantly more stable than the one terminated with PDADMAC and chitosan, respectively, implying cross-linking properties of heparin. Evaluation of OWLS, AFM, and QCM-D data provides valuable insights into the formation and structure of those macroion films. Stronger electrostatic interactions within (PDADMAC/heparin) multilayers lead to the assembly of stable, homogeneous, and rigid films, whereas (chitosan/heparin) films were less stable against rinsing, softer and possess a higher swelling capacity. Those conclusions were verified using AFM imaging in the liquid of respective assemblies. Collected topography mappings of wet $(PDADMAC/heparin)_5$ film confirmed a homogenous plane layer, although wet $(chitosan/heparin)_5$ film images revealed heterogenous nanofibril/spongy structure with uncovered substrate regions. The formation of stable and rigid PDADMAC/heparin films was explained by the effective creation of ion-pair complexes between oppositely charged strong macroions. On the other hand, the interactions between weak chitosan and strong heparin were significantly weaker, leading to softer, more hydrated quasi-gel films, exhibiting nonlinear growth.

Apart from its undoubted advantages, the applied experimental methods also have several disadvantages. Correction for surface conductivity should be undertaken if the measurements are carried out at low ionic strength and thin channels in SPM. Furthermore, assembling the SP cell is tedious and time-consuming and the side walls can be made of different materials than the basal walls. On the other hand, OWLS technique cannot be used with opaque substrates because it relies on the assumption of a homogeneous layer and an isotropic refractive index. While OWLS uses both TE and TM polarisations, RWG employs the TM polarization only, making impossible to independently measure both layer thickness and refractive index when thin adlayers are measured. Concerning cell adhesion, RWG records the adhesion force of living cells

indirectly, its calibration was conducted only recently (Sztilkovics). It is also important to note that the employed DH setup has a strong limitation in resolving very thin parts of the adhered cells, but it is ideal to measure cellular movements [43]. In case of AFM measurements, special attention must be paid to controlling the loading forces to minimize sample deformation or damage as well as the generation of artifacts. Moreover, the resolution of an AFM microscope is limited by the tip radius. Sharp AFM probes provide high resolution but are more likely to be damaged during scanning, which may result in overestimation of the size of the scanned objects.

The RWG real-time monitoring disclosed that (PDADMAC/heparin)$_3$PDADMAC multilayers strongly affected the cell adhesion, whereas it was negligible on (chitosan/heparin)$_5$ multilayers. Accordingly, one can state that the murine preosteoblastic cells adhere more easily to the positively charged, homogeneous, and rigid macroion films. Furthermore, multilayers with positively charged top layer allow for a more pronounced cell spreading as was confirmed by digital holographic microscopy. The significant cell attachment and spreading could be explained by strong electrostatic interactions that occurred between the negatively charged cell membrane and positively charged substrate.

Hereby characterized films constitute a scaffold for effective preosteoblast adhesion and spreading. In the future, these polysaccharide-based multilayers can be considered as versatile systems for medical applications such as immunomodulation therapy, tissue engineering, and antimicrobial coatings for medical devices.

Declaration of competing interest

The authors declare the following financial interests/personal relationships which may be considered as potential competing interests: Aneta Michna reports financial support was provided by National Science Centre Poland.

Acknowledgments

This work was financially supported by the National Science Centre, Poland, Opus Project, 2018/31/B/ST8/03277.

M.W. would like to thank the European Union Erasmus + Programme (project no: 2020-1-PL01-KA103-078621) for providing financial support for the mobility and training in Nanobiosensoric Laboratory in Budapest to perform Epic BT and HoloMonitor studies.

The biological part was supported by the Hungarian Academy of Sciences [Lendület (Momentum) Program], the National Research, Development, and Innovation Office (NKFIH) [KKP 129936 and TKP2021-EGA-04 Programs and PD grant 134195 for Z.Sz].

Appendix A. Supplementary data

Supplementary data to this article can be found online at https://doi.org/10.1016/j.ijbiomac.2023.125701.

References

[1] S.-H. Kim, J. Turnbull, S. Guimond, Extracellular matrix and cell signaling: the dynamic cooperation of integrin, proteoglycan and growth factor receptor, J. Endocrinol. 209 (2011) 139–151.
[2] S. Malagobadan, N. Hasima Nagoor, Anoikis, in: Encyclopedia of Cancer, Third Edition, 2019.
[3] M.L. Taddei, E. Giannoni, P. Fiaschi, P. Chiarugi, Anoikis: an emerging hallmark in health and diseases, J. Pathol. 226 (2012) 380–393.
[4] R. Orgovan, B. Peter, S. Bősze, J.J. Ramsden, B. Szabó, R. Horvath, Dependence of cancer cell adhesion kinetics on integrin ligand surface density measured by a high-throughput label-free resonant waveguide grating biosensor, Sci. Rep. 4 (2014) 4034.
[5] J.J. Ramsden, R. Horvath, Optical biosensors for cell adhesion, Journal of Receptors and Signal Transduction 29 (3–4) (2009) 211–223.
[6] P. Tryoen-Toth, D. Vautier, Y. Haikel, J. Voegel, P. Schaaf, J. Chluba, J. Ogier, Viability, adhesion, and bone phenotype of osteoblast-like cells on polyelectrolyte multilayer films, J. Biomed. Mater. Res. 60 (2002) 657–667.
[7] C. Boura, P. Menu, E. Payan, C. Picart, J. Voegel, S. Muller, J. Stoltz, Endothelial cells grown on thin polyelectrolyte multilayered films: an evaluation of a new versatile surface modification, Biomaterials 24 (2003) 3521–3530.
[8] B. Purohit, P.R. Vernekar, N.P. Shetti, P. Chandra, Biosensor nanoengineering: design, operation, and implementation for biomolecular analysis, Sensors International 1 (2020), 100040.
[9] P. Chandra, R. Prakash, Nanobiomaterial Engineering. Concepts and Their Applicationx in Biomedicine and Diagnostics, Springer, 2020.
[10] S.N. Joshi, P. Chandra, Advanced Micro- and Nano-manufacturing Technologies. Applications in Biochemical and Biomedical Engineering, Springer, 2022.
[11] D.P. Reyes, E.M. Perruccio, S.P. Becerra, L.E. Locascio, M. Gaitan, Micropatterning neuronal cells on polyelectrolyte multilayers, Langmuir 20 (2004) 8805–8811.
[12] D.L. Elbert, C.B. Herbert, J.A. Hubbell, Thin polymer layers formed by polyelectrolyte multilayer techniques on biological surfaces, Langmuir 15 (1999) 5355–5362.
[13] J.D. Mendelsohn, S.Y. Yang, J. Hiller, A.I. Hochbaum, M.F. Rubner, Rational design of cytophilic and cytophobic polyelectrolyte multilayer thin films, Biomacromolecules 4 (2003) 96–106.
[14] Reichert, L., Schneider, A., Vautier, D., Vodouhe, C., Jessel, N., Paycen, E., Schaaf, P., Voegel, J-C., Picart, C., Imaging cell interactions with native and crosslinked polyelectrolyte multilayers. Cell Biochem. Biophys. 2006, 44, 273–285.
[15] G.V. Martins, E.G. Merino, J.F. Mano, N.M. Alves, Crosslink effect and albumin adsorption onto chitosan/alginate multilayered systems: an in situ QCM-D study, Macromol. Biosci. 10 (2010) 1444–1455.
[16] J. Lyklema, Fundamentals of Interface and Colloid Science V: Soft Colloids, Academic Press, San Diego, 2005.
[17] G. Decher, J.D. Hong, J. Schmitt, Buildup of ultrathin multilayer films by a self-assembly process: III. Consecutively alternating adsorption of anionic and cationic polyelectrolytes on charged surfaces, Thin Solid Films 210 (211) (1992) 831–835.
[18] M. Bulwan, K. Wójcik, S. Zapotoczny, M. Nowakowska, Chitosan-based ultrathin films as antifouling, anticoagulant and antibacterial protective coatings, Journal of Biomaterial Science 23 (2012) 1963–1980.
[19] J.J. Richardson, et al., Innovation in layer-by-layer assembly, Chem. Rev. 116 (2016) 14828–14867.
[20] S. Pahal, R. Gakhar, A.M. Raichur, M.M. Varma, Polyelectrolyte multilayers for bioapplications: recent advancements, IET Nanobiotechnol 11 (2017) 903–908.
[21] P.J. Rivero, J. Goicoechea, F.J. Arregui, Layer-by-layer nano-assembly: a powerful tool for optical fibre sensing applications, Sensors 19 (2019) 683.
[22] J. Campbell, A.S. Vikulina, Layer-by-layer assemblies of biopolymers: build-up, mechanical stability, and molecular dynamics, Polymers (Basel) 12 (2020) 1949.
[23] V. Gejji, S. Fernando, Polyelectrolyte based technique for sequestration of protein from an aqueous phase to an organic solvent, Sep. Purif. Technol. 207 (2018) 68–76.
[24] S. Wang, K. Chen, Y. Xu, X. Yu, W. Wang, L. Li, X. Guo, Protein immobilization and separation using anionic/cationic spherical polyelectrolyte brushes based on charge anisotropy, Soft Matter 9 (2013) 11276–11287.
[25] X. Zhao, Y. Zhang, Bacteria-removing and bactericidal efficiencies of PDADMAC composite coagulants in enhanced coagulation treatment, Clean 41 (2013) 37–42.
[26] A. Baranwal, A. Kumar, A. Priyadharshini, G.S. Oggu, I. Bhatnagar, A. Srivastava, P. Chandra, Chitosan: an undisputed bio-fabrication material for tissue engineering and biosensing applications, Int. J. Biol. Macromol. 110 (2018) 110–123.
[27] R.C.F. Cheung, T.B. Ng, J.H. Wong, W.Y. Chan, Chitosan: an update on potential biomedical and pharmaceutical applications, Mar Drugs 13 (2015) 5156–5186.
[28] L. Gibot, S. Chabaud, S. Bouhout, S. Bolduc, F.A. Auger, V.J. Moulin, Anticancer properties of chitosan on human melanoma are cel line dependent, Int. J. Biol. Macromol. 72 (2015) 370–379.
[29] Y. Zhou, D. Yang, X. Chen, Q. Xu, F. Lu, J. Nie, Electrospun water-soluble carboxyethyl chitosan/poly(vinyl alcohol) nanofibrous membrane as potential wound dressing for skin regeneration, Biomacromolecules 9 (2008) 349–354.
[30] U. Lindahl, M. Kusche-Gullberg, L. Kjellen, Regulated diversity of Heparan sulfate, J. Biol. Chem. 273 (1998) 24979–24982.
[31] M. Salmivirta, K. Lidholt, U. Lindahl, Heparan sulfate: a piece of information, FASEB J. 10 (1996) 1270–1279.
[32] J. Hirsh, T.E. Warkentin, S.G. Shaughnessy, S. Anand, J.L. Halperin, R. Raschke, C. Granger, E.M. Ohman, J.E. Dalen, Heparin and low-molecular-weight heparin., Mechanism of action, pharmacokinetics, dosing, monitoring, efficacy, and safety, Chest 119 (2001) 64S–94S.
[33] I. Capila, R.J. Linhardt, Heparin – protein interactions, Angew. Chem. Int. Ed. 41 (2002) 390–412.
[34] S.J. Paluck, T.H. Nguyen, H.D. Maynard, Heparin-mimicking polymers: synthesis and biological applications, Biomacromolecules 17 (2016) 3417–3440.
[35] L. Benington, G. Rajan, C. Locher, L.Y. Lim, Fibroblast growth factor 2 – a review of stabilization approaches for clinical applications, Pharmaceutics 12 (2020) 508.
[36] L.D. Shea, D. Wang, R.T. Franceschi, D.J. Mooney, Engineered bone development from a pre-osteoblast cell line on three-dimensional scaffolds, Tissue Eng. 6 (2000) 605–617.
[37] P. Arpornmaeklong, N. Suwatwirote, P. Pripatnanont, K. Oungbho, Growth, and differentiation of mouse osteoblasts on chitosan-collagen sponges, Int. J. Oral Maxillofac. Surg. 36 (2007) 328–337.
[38] W. Suphasiriroj, P. Yotnuengnit, R. Surarit, R. Pichyangkura, The fundamental parameters of chitosan in polymer scaffolds affecting osteoblasts (MC3T3-E1), J. Mater. Sci. Mater. Med. 20 (2009) 309–320.
[39] J.W. Calvert, W.C. Chua, N.A. Gharibjanian, S. Dhar, G.R.D. Evans, Osteoblastic phenotype expression of MC3T3-E1 cells cultured on polymer surfaces, Plastic and Reconstructive Surgery 116 (2005) 567–576.

[40] Orgovan, R., Kovacs, B., Farkas, E., Szabo, B., Zaytseva, N., Fang, Y., Horvath, R. Bulk and surface sensitivity of a resonant waveguide grating imager. Appl. Phys. Lett., 2014, 104(8), 083506–083506-4.
[41] B. Peter, E. Farkas, E. Forgacs, A. Saftics, B. Kovacs, S. Kurunczi, I. Szekscs, A. Csampai, S. Bosze, R. Horvath, Green tea polyphenol tailors cel adhesivity of RGD displaying surfaces: multicomponent models monitored optically, Sci. Rep. 7 (2017) 42220.
[42] M. Sztilkovics, T. Gerecsei, B. Peter, A. Saftics, S. Kurunczi, I. Szekscs, B. Szabó, R. Horvath, Single-cell adhesion force kinetics of cell populations from combined label-free optical biosensor and robotic fluidic force microscopy, Sci. Rep. 10 (2020) 61.
[43] B. Peter, J. Nador, K. Juhasz, A. Dobos, L. Korosi, I. Szekacs, D. Patko, R. Horvath, Incubator proof miniaturized Holomonitor to in situ monitor cancer cells exposed to green tea polyphenol and preosteoblast cells adhering on nanostructured titanate surfaces: validity of the measured parameters and their corrections, J. Biomedical Optics 20 (2015), 067002.
[44] D. Lupa, W. Płaziński, A. Michna, M. Wasilewska, P. Pomastowski, A. Gołębiowski, B. Buszewski, Z. Adamczyk, Chitosan characteristics in electrolyte solutions: combined molecular dynamics modeling and slender body hydrodynamics, Carbohydr. Polym. 292 (2022), 119676.
[45] M.J. Bof, V.C. Bordagaray, D.E. Locaso, M.A. Garcia, Chitosan molecular weight effect on starch-composite film properties, Food Hydrocoll. 51 (2015) 281–294.
[46] W. Tachaboonyakiat, T. Serizawa, T. Endo, et al., The influence of molecular weight over the ultrathin films of biodegradable poluion complexes between chitosan and poly(γ-glutamic acid), Polym. J. 32 (2000) 481–485.
[47] S.Y. Park, K.S. Marsh, J.W. Rhim, Characteristics of different molecular weight chitosan films affected by the type of organic solvents, J. Food Sci. 67 (2002) 194–197.
[48] Y. Zhong, C. Zhuang, W. Gu, Y. Zhao, Effect of molecular weight on the properties of chitosan films prepared using electrostatic spraying technique, Carbohydr. Polym. 212 (2019) 197–205.
[49] A. Michna, A. Pomorska, M. Nattich-Rak, M. Wasilewska, Z. Adamczyk, Hydrodynamic solvation of poly (amido amine) dendrimer monolayers on silica, J. Phys. Chem. C 124 (2020) 17684–17695.
[50] A. Michna, J. Maciejewska-Prończuk, A. Pomorska, M. Wasilewska, T. Kilicer, J. Witt, O. Ozcan, Effect of the anchoring layer and transport type on the adsorption kinetics of lambda carrageenan, J. Phys. Chem. B 125 (2021) 7797–7808.
[51] M. von Smoluchowski, Contribution to the theory of electro-osmosis and related phenomena, Bull. Int. L'Acadèmie Sci. Cracovie 3 (1903) 182–199.
[52] J. Vörös, J. Ramsden, G. Csúcs, I. Szendrő, S.M. De Paul, M. Textor, N.D. Spencer, Optical grating coupler biosensors, Biomaterials 23 (2002) 3699–3710.
[53] A. Saftics, S. Kurunczi, B. Peter, I. Szekacs, J.J. Ramsden, R. Horvath, Data evaluation for surface-sensitive label-free methods to obtain real-time kinetic and structural information of thin films: a practical review with related software packages, Adv. Colloid Interf. Sci. 294 (2021), 102431.
[54] J.A. De Feijter, J. Benjamins, F.A. Veer, Ellipsometry as a tool to study the adsorption behavior of synthetic and biopolymers at the air−water interface, Biopolymers 17 (1978) 1759–1772.
[55] M. Wasilewska, Z. Adamczyk, M. Sadowska, F. Boulmedais, M. Cieśla, Mechanisms of fibrinogen adsorption on silica sensors at various pHs: experiments and theoretical modeling, Langmuir 35 (2019) 11275–11284.
[56] A. Pomorska, Z. Adamczyk, M. Nattich-Rak, M. Sadowska, Kinetics of human serum albumin adsorption at silica sensor: unveiling dynamic hydration function, Colloids Surf. B: Biointerfaces 167 (2018) 377–384.
[57] B. Peter, R. Ungai-Salanki, B. Szabo, A.G. Nagy, I. Szekacs, S. Bősze, R. Horvath, High-resolution adhesion kinetics of EGCG-exposed tumor cells on biomimetic interfaces: comparative monitoring of cell viability using label-free biosensor and classic ned-point assay, ACS Omega 3 (2018) 3882–3891.
[58] Wu Chung-Hsin, Xin-Ji Lai, Chau-Jern Cheng, Yu Yu-Chen, Chun-Yen Chang, Applications of digital holographic microscopy in therapeutic evaluation of Chinese herbal medicines, Appl. Opt. 53 (2014) G192–G197.
[59] B. Janicke, A. Kårsnäs, P. Egelberg, K. Alm, Label-free high temporal resolution assessment of cell proliferation using digital holographic microscopy, Cytometry 91 (2017) 460–469.
[60] Y. Zhang, R.L. Judson, Evaluation of holographic imaging cytometer holomonitor M4® motility applications, Cytometry 93 (2018) 1125–1131.
[61] M. Hellesvik, H. Øye, H. Aksnes, Exploiting the potential of commercial digital holographic microscopy by combining it with 3D matrix cell culture assays, Sci. Rep. 10 (2020) 14680.
[62] K.M. Eder, A. Marzi, Á. Barroso, S. Ketelhut, B. Kemper, J. Schnekenburger, Label-free digital holographic microscopy for in vitro cytotoxic effect quantification of organic nanoparticles, Cells 11 (2022) 644.
[63] M. Morga, A. Michna, Z. Adamczyk, Formation and stability of polyelectrolyte/polypeptide monolayers determined by electrokinetic measurements, Colloids Surf. A Physicochem. Eng. Asp. 529 (2017) 302–310.
[64] M.R. Kreke, A.S. Badami, J.B. Brady, R.M. Akers, A.S. Goldstein, Modulation of protein adsorption and cell adhesion by poly(allylamine hydrochloride) heparin films, Biomaterials 26 (2005) 2975–2981.
[65] M. Yu, T. Zhang, J.P. Li, Y. Tan, Elucidating the binding mode between heparin and inflammatory cytokines by molecular modeling, ChemistryOpen 10 (2021) 966–975.
[66] G. Zhou, M.S. Niepel, S. Saretia, T. Groth, Reducing the inflammatory responses of biomaterials by surface modification with glycosaminoglycan multilayers, J. Biomed. Mater. Res. A 104 (2016) 493–502.
[67] Y. Lim, S.Y. Lee, Capacitance measurement of SiO2@ BSA Core-Shell nanoparticles using AC impedance spectroscopy, J. Electrochem. Soc. 162 (2015) G48.
[68] T.D. Andreeva, A. Der, L. Kelemen, R. Krastev, S. Taneva, Modulation of the internal structure and surface properties of natural and synthetic polymer matrices by graphene oxide doping, Polym. Adv. Technol. 31 (2020) 1562–1570.
[69] F. Boulmedais, C.S. Tang, B. Keller, J. Vörös, Controlled electrodissolution of polyelectrolyte multilayers: a platform technology towards the surface-initiated delivery of drugs, Adv. Funct. Mater. 16 (2006) 63–70.
[70] M. Morga, Z. Adamczyk, D. Kosior, M. Kujda-Kruk, Kinetics of poly-L-lysine adsorption on mica and stability of formed monolayers: theoretical and experimental studies, Langmuir 35 (2019) 12042–12052.
[71] N. Orgovan, R. Ungai-Salánki, S. Lukácsi, N. Sándor, Z. Bajtay, A. Erdei, B. Szabó, R. Horvath, Adhesion kinetics of human primary monocytes, dendritic cells, and macrophages: dynamic cell adhesion measurements with a label-free optical biosensor and their comparison with end-point assays, Biointerphases 11 (2016), 031001.
[72] K.D. Kovács, M. Novák, Z. Hajnal, C. Hős, B. Szabó, I. Székács, Y. Fang, A. Bonyár, R. Horvath, Label-free tracking of whole-cell response on RGD functionalized surfaces to varied flow velocities generated by fluidic rotation, J. Colloid Interface Sci. 599 (2021) 620–630.
[73] N. Kanyo, K.D. Kovacs, A. Saftics, B. Peter, A.R. Santa-Maria, F.R. Walter, A. Dér, M.A. Deli, R. Horvath, Glycocalyx regulates the strength and kinetics of cancer cell adhesion revealed by biophysical models based on high resolution label-free optical data, Sci. Rep. 10 (2020) 22422.
[74] R.I. Freshney, Culture of Animal Cells: A Manual of Basic Technique, 4th ed., Wiley-Liss, New York, 2000 (Ch. 2).
[75] L. Richert, P. Lavalle, E. Payan, X.Z. Shu, G.D. Prestwich, J.F. Stoltz, P. Schaaf, J. C. Voegel, C. Picart, Layer by layer buildup of polysaccharide films: physical chemistry and cellular adhesion aspects, Langmuir 20 (2004) 448–458.